Fractional quantum Hall nematics at $\nu = \frac{7}{3}$ in a tilted magnetic field

Dan Ye, Chen-Xin Jiang, and Zi-Xiang Hu*
Department of Physics and Chongqing Key Laboratory for Strongly Coupled Physics, Chongqing University, Chongqing 401331, People's Republic of China

(Received 24 March 2024; revised 24 September 2024; accepted 26 September 2024; published 9 October 2024)

We investigated the behavior of fractional quantum Hall (FQH) states in a two-dimensional electron system with layer thickness and an in-plane magnetic field. Our comparisons across various filling factors within the first Landau level revealed a crucial observation. A slight in-plane magnetic field specifically enhances the nematic order of the $\nu = 7/3$ FQH state. For this particular filling, through calculating the energy gap, the Ising nematic order parameter, the pair-correlation function, and the static structure factor, we observed that as the in-plane magnetic field increases, the system started from the isotropic FQH (IFQH) state, first enters into an anisotropic FQH (AFQH) phase without closing the spectrum gap, then the FQH nematic (FQHN) phase after neutral gap closing. The system eventually enters a gapless one-dimensional charge density wave (CDW) phase for a large in-plane field. We thus provide a full phase diagram of the $\nu = 7/3$ state in a tilted magnetic field, demonstrating the existence of the FQHN, which aligns with recent resonant inelastic light scattering experimental observations.

DOI: 10.1103/PhysRevB.110.165123

I. INTRODUCTION

The fractional quantum Hall effect remains one of the most interesting strongly correlated systems for electrons moving in an effective two-dimensional manifold [1,2]. Generally speaking, the ground states of the fractional quantum Hall (FQH) liquid are incompressible with topological order, that is, order without dependence on any symmetries [3]. Additionally, spontaneous breaking of symmetry within the FQH liquid can potentially give rise to electronic liquid crystal phases, such as nematic, smectic, and stripe order [4–12]. A particular area of interest arises when these distinct phases coexist, leading to quantum liquid crystal phases like fractional quantum Hall nematic phases. The concept of fractional quantum Hall nematic effect (FQHN) was originally proposed by Balents [13] which was recently discovered in experiments [14,15]. These phases have been experimentally observed in transport measurements [16]. By manipulating factors such as the in-plane magnetic field [17,18], valley occupancy through application of in-plane strain [19–21] or magnetoresistance measurements under hydrostatic pressure [22–24] researchers have observed systems exhibiting anisotropic longitudinal resistivity that is enhanced at low temperatures, along with a robust Hall conductivity plateau. The nematic state is fully translationally invariant, but lacks rotational invariance. It can be visualized as stripes that fluctuate strongly and are riddled with dislocation defects but retain a preferential alignment in one direction. To definitively confirm the existence of a nematic phase, it is crucial to simultaneously investigate both rotational symmetry and translational invariance. However, previous studies have mainly focused on the breaking of rotational symmetry without achieving long-range translational invariance. Only recently, with the work reported in Ref. [25], there has been simultaneous evidence of coexistence of broken rotational symmetry and translational invariance, allowing the identification of nematic phases.

Theoretical investigations, including the Hartree-Fock approximation and effective field theories, have predicted a range of phases in addition to the expected Wigner crystals. These include stripe phases, bubble phases, and other crystalline states [26–31]. These predictions have been further elaborated upon by various field theory approaches, which describe the incompressible nematic phase using an effective gauge theory [32,33] or by assuming the softening of the magnetoroton mode [34,35]. These theories aim to capture the topological order and the nematic order resulting from spontaneous symmetry breaking. Microscopic theories, on the other hand, focus on analyzing the microscopic properties of FQHN in the thermodynamic limit, providing the necessary conditions for the robustness of the nematic fractional quantum Hall effect in microscopic Hamiltonians [36]. Recent numerical studies have further supported the existence of FQHN phases in both bosonic and fermionic systems, with the tuning of pseudopotential coefficients in a model Hamiltonian [37–39].

The FQH states within the first Landau level (1LL) exhibit smaller energy gaps and are generally more prone to perturbations compared to those found in the lowest Landau level (LLL), as documented in various studies [40–44]. Consequently, the spontaneous emergence of nematic order, which involves the spontaneous breaking of rotational symmetry without a preferred direction, may be more feasible in higher LLs due to the reduced energetic barrier required for its stabilization. FQH states exhibit inconsistent responses depending on the filling factor. At half-filling $\nu = 5/2$, the ground state is described as a p-wave paired superfluid, as supported by numerous studies [45–48]. However, in the presence of a sufficiently large in-plane magnetic

*Contact author: zxhu@cqu.edu.cn

field, the 5/2 FQH state transitions into a compressible nematic phase [16,42,49–51]. On the other hand, at $\nu = 7/3$, the application of even small in-plane magnetic fields leads to a pronounced transport anisotropy that coexists with the quantized Hall plateau, indicating the existence of the FQH nematic [14]. To investigate the FQH nematic phase at various filling factors within the 1LL, we utilize torus geometry with periodic boundary condition in two main directions to detect translational symmetry. The introduction of an in-plane magnetic field to the electrons introduces anisotropy, thereby disrupting the rotational symmetry of the system. Recently, one of us generalized the description of pseudopotentials to incorporate nonzero off-diagonal pseudopotentials $v_{m,n}$ (where $m \neq n$) that do not conserve angular momentum conservation. This generalization enables the representation of system anisotropy in the absence of rotational invariance [52,53].

In this work, we present a microscopic study in a realistic model examining the influence of in-plane magnetic field and layer thickness on FQH states within the 1LL, across different filling factors, especially at $\nu = 7/3$. The analysis is grounded in the pseudopotential description of electron-electron interaction within an in-plane magnetic field, accounting for finite layer thickness. The paper is organized as follows. Section II reviews the single-electron solution, delves into the pseudopotentials, and analyzes their behavior with varying parameters. Section III provides the primary result of this work, the phase diagram of the 7/3 state as a function of in-plane field and layer thickness in advance. The numerical evidences of the different phases are given by calculating the Ising nematic order, wave function overlap, energy gap, correlation function and structure factor. Finally, Sec. IV concludes the article with a summary of our findings.

II. MODEL AND METHOD

We explore the impacts of a tilted magnetic field that has a component perpendicular to the plane ($B_\perp$) and a component within the plane ($B_\parallel$). Without loss of generality, we assume that the in-plane field $B_\parallel$ is oriented along the x axis. In particular, the in-plane magnetic field $B_\parallel$ influences the system only when the thickness of the two-dimensional electron gases is significant. For simplicity, we consider the electrons to be confined in the z direction by a parabolic quantum well potential represented by $\frac{1}{2}m_e\tilde{\omega}_0 z^2$. The thickness of the system is related to the characteristic width of the harmonic well, defined as $\omega_0 = 1/\sqrt{m_e\tilde{\omega}_0}$, in which m_e denotes the effective mass of the electrons and $\tilde{\omega}_0$ is the angular frequency associated with the confinement potential in the z direction. This assumption allows us to simplify the problem by focusing solely on the electron motion within the plane, while incorporating the finite thickness of the system through the parameter ω_0. The single-particle Hamiltonian is then expressed as

$$H = \frac{1}{2m_e}\sum_{i=x,y,z}(p_i + eA_i)^2 + \frac{1}{2}m_e\tilde{\omega}_0^2 z^2, \tag{1}$$

Similar to the special case where $B_\parallel$ is absent, the Hamiltonian can be expressed in a diagonal form as

$$H = \omega_1 X^\dagger X + \omega_2 Y^\dagger Y + \text{constant}, \tag{2}$$

where $(X, X^\dagger)$ and $(Y, Y^\dagger)$ are two sets of decoupled bosonic operators obeying the canonical commutation relation $[X, X^\dagger] = [Y, Y^\dagger] = 1$ and $[X, Y] = 0$. They are linear combinations of the canonical momentums, where $\pi_i = p_i + eA_i$ for $i = 1, 2, 3$, and $\pi_4 = m_e\tilde{\omega}_0 z$. The details of the diagonalization procedure can be found in Ref. [54]. The quasiparticle eigenenergy is given by $\omega_1^2 = \frac{1}{2}(\tilde{\omega}_0^2 + \omega_x^2 + \omega_z^2 - \sqrt{-4\tilde{\omega}_0^2\omega_z^2 + (\tilde{\omega}_0^2 + \omega_x^2 + \omega_z^2)^2})$, $\omega_2^2 = \frac{1}{2}(\tilde{\omega}_0^2 + \omega_x^2 + \omega_z^2 + \sqrt{-4\tilde{\omega}_0^2\omega_z^2 + (\tilde{\omega}_0^2 + \omega_x^2 + \omega_z^2)^2})$. Here, ω_x and ω_z represent the cyclotron frequencies corresponding to $eB_\parallel/m_e$ and $eB_\perp/m_e$, respectively. As a result, the single-particle Landau wave functions are now indexed by two quantum numbers $|l, t\rangle = \frac{1}{\sqrt{l!t!}}(X^\dagger)^l(Y^\dagger)^t|0\rangle$, where $|0\rangle$ is the vacuum state. In the limit of $\omega_x \to 0$, when $\tilde{\omega}_0 > \omega_z$, the operator $(X, X^\dagger)$ raises and lowers the in-plane Landau levels, while the operator $(Y, Y^\dagger)$ raises and lowers the harmonic modes along the z axis (or the subbands). The roles of X and Y are reversed for $\tilde{\omega}_0 < \omega_z$. More details could be found in Ref. [54].

The three-dimensional Coulomb interaction has the Fourier form $V_{\vec{k}} = 1/k^2 = 1/(|\vec{q}|^2 + q_3^2)$ where $\vec{q}$ is the two-dimensional vector. Its LLL projected Hamiltonian is

$$H_C = \int d^3k V_{\vec{k}}|F_{lt}(\vec{q}, q_3)|^2\hat{\rho}_{\mathbf{q}}\hat{\rho}_{-\mathbf{q}}e^{-q^2/2}, \tag{3}$$

where $\hat{\rho}_{\mathbf{q}} = \sum_i e^{i\vec{q}\cdot\mathbf{r}_i}$ is the guiding center density and $F_{l,t}(\vec{q}, q_3)$ is the form factor from the LLL projection. The lowest LL is defined as $l = t = 0$ and the 1LL is for $l = 0, t = 1$ or $l = 1, t = 0$. After integrating the z component q_3, we thus obtain the effective 2D interaction [44,54]:

$$V_{\text{eff}}(\vec{q}) = \int_{-\infty}^{\infty} dq_3 \frac{1}{|\vec{q}|^2 + q_3^2}|F_{lt}(\vec{q}, q_3)|^2. \tag{4}$$

For a two-body interaction without rotational symmetry, the matrix element of the pseudopotential coefficient is expressed as $\langle m|H_C|m'\rangle$ where $|m\rangle$ is the two-body wave function with relative angular momentum m. It was found [53] that a generalized pseudopotential description can be used to describe it:

$$\begin{aligned}\Gamma^+_{m,n}(\mathbf{k}) &= \lambda_n\mathcal{N}_{mn}\left(L_m^n(|k|^2)e^{-|k|^2/2}\mathbf{k}^n + \text{c.c.}\right),\\ \Gamma^-_{m,n}(\mathbf{k}) &= -i\mathcal{N}_{mn}\left(L_m^n(|k|^2)e^{-|k|^2/2}\mathbf{k}^n - \text{c.c.}\right),\end{aligned} \tag{5}$$

where $\mathcal{N}_{mn}$ is the normalization factors, $n = m - m'$. The effective two-body interaction including the anisotropic one can be expanded as $V_{\text{eff}}(\mathbf{k}) = \sum_{m,n,\sigma}^{\infty} v_{m,n}^\sigma\Gamma_{m,n}^\sigma(\mathbf{k})$ with coefficient $v_{m,n}^\sigma = \int d^2k V_{\text{eff}}(\mathbf{k})\Gamma_{m,n}^\sigma(\mathbf{k})$. For $n = 0$, the generalized pseudopotential can be returned to the isotropic Haldane pseudopotential, namely $\Gamma_{m,0}^+ = \Gamma_m$, $\Gamma_{m,0}^- = 0$ and $v_{m,0}^+ = v_m$, $v_{m,0}^- = 0$.

In Fig. 1, we display the ratio of the effective interactions along the q_x and q_y axes on a circle with a radius of q, considering various strengths of the parallel magnetic field with a fixed layer thickness. In particular, when ω_x is nonzero, the strength of the effective interaction exhibits anisotropy, with a ratio different from one. This anisotropy leads to a break of the rotational symmetry. Furthermore, as ω_x increases, the ratio changes from being greater than one to smaller than one, indicating a potential change in the orientation of

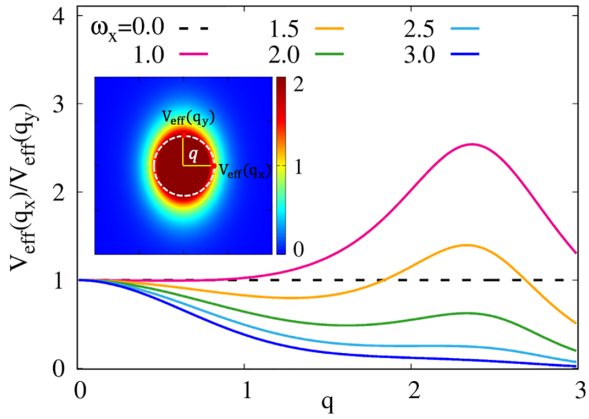

FIG. 1. Given a layer thickness at $\omega_0 = 1.25$, the ratio of effective interaction in two directions as a function of the circular radius q at different ω_x. The inset is the 2D distribution of $V_{\text{eff}}(\vec{q})$ at $\omega_x = 3.0$.

the effective interaction anisotropy. Such anisotropies can be experimentally probed through measurements related to the ground-state structure factor and the neutral excitation gap, providing valuable insight into the physics of the system. It is known that the model Hamiltonian contains only v_1 interaction has the Laughlin wave function [3] as the densest zero-energy eigenstate. Therefore, in a realistic model with Coulomb interaction, the relative value of v_1 compared to other pseudopotentials plays a crucial role in stabilizing the Laughlin state in 1/3 filling. Figure 2(a) illustrates the pseudopotential coefficients v_1/v_3 on a 2D graph while changing the values of ω_x and ω_0. We can see that v_1/v_3 exhibits a peak value ($v_1/v_3 \sim 1.5$ compared to the Coulomb value 1.32) at a finite ω_x, indicating that a finite in-plane magnetic field tends to stabilize the Laughlin state at $\nu = 7/3$. This phenomenon is also evident in the energy gap as shown below. It has previously been verified by experiment [55] in which a

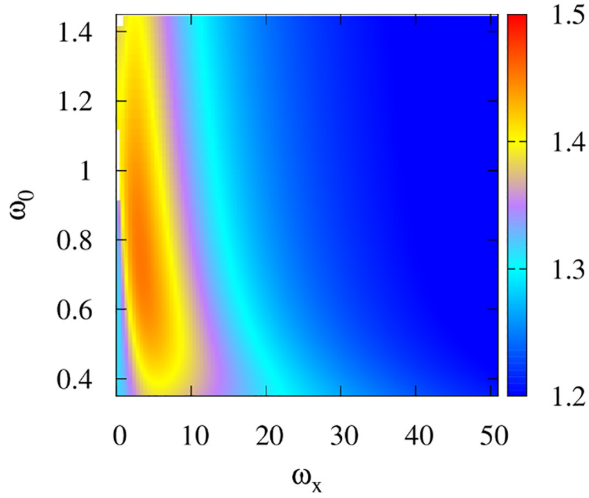

FIG. 2. The ratio of v_1/v_3 reaches a peak at finite ω_0 and ω_x. The peak value is around $v_1/v_3 \sim 1.5$, which is higher than the pure Coulomb value of 1.32 in the 1LL when the layer thickness is not considered, indicating an increase in the gap at finite ω_0 and ω_x.

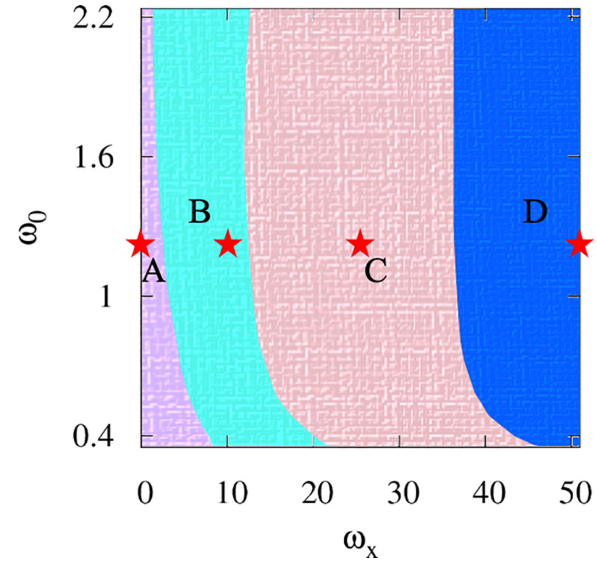

FIG. 3. Schematic phase diagram labeled by A: IFQH, B: AFQH, C: FQHN and D: CDW, respectively. A representative point in each phase, marked by stars, is chosen to demonstrate the physical properties in the numerical analysis.

strong enhancement of the gap was observed in a wide 2D quantum well.

III. NUMERICAL RESULTS

We consider a system with N_e electrons in the torus geometry. The number of quantum fluxes N_ϕ fixes the filling factor $\nu = N_e/N_\phi$. The torus is spanned by the vectors $\hat{L}_x$ and $\hat{L}_y$ in two principle directions. Unless otherwise specified, we consider a rectangle torus with 90 degrees angle between $\hat{L}_x$ and $\hat{L}_y$. The aspect ratio $L_x/L_y = 1$ is set mainly at unity. For $N_e = pN$ particles in $N_\phi = qN$ orbits with a maximum common divisor N, the filling factor is $\nu = p/q$. The many-body center-of-mass magnetic translation operator $\bar{T}(a) = \prod_{i=1}^{N_e} T_i(a)$ in which $T_i(a)$ is the magnetic translation operator for each electron. In Landau gauge, we have two good quantum numbers $t = \sum_{i=1}^{N_e} m_i \bmod N_\phi$, the total momentum in the y direction in units of $2\pi/L_y$, and s, the center of mass translational momentum in units of $2\pi/L_x$ which contributes the q-fold degeneracy in energy spectrum. That is, they obey the relation $\bar{T}(L_x/N) = e^{i2\pi s/N}$ and $\bar{T}(L_y/N) = e^{i2\pi t/N}$.

To begin with, we aim to present the primary outcome of this work as depicted in Fig. 3 prior to detailing the numerical evidence. Generally, we identify four phases at $\nu = 7/3$ by adjusting the parameters ω_0 and ω_x. The isotropic FQH phase (A) which conserves both rotational symmetry and translational symmetry, is decided by its overlap with the isotropic Laughlin wave function. The anisotropic FQH phase (B) has nonzero Ising nematic order, a finite energy gap in $k = 0$ space, and an optimizable overlap with the generalized Laughlin wave function. The FQHN phase (C) is characterized by nonzero Ising nematic order and gap closing in thermodynamic limit. Finally, the charge density wave (CDW) phase (D) is characterized by zero nematic order, zero energy

gap, and two pronounced peaks in the static structure factor. We select specific values for the parameters ω_0 and ω_x at a representative point in each phase, indicated by asterisks in Fig. 3, to illustrate these physical characteristics in the subsequent discussion.

A. Ising nematic order

The nematic phase is translationally invariant, but breaks rotational invariance. Their order parameters undergo irreducible transformations under the rotation group of the continuous system or the point group of the lattice. Therefore, the order parameters of the nematic phase are trace-free symmetric tensors, which we represent as Q_{ij}. In two dimensions, $Q_{ij} = \begin{pmatrix} Q_{xx} & Q_{xy} \\ Q_{xy} & -Q_{xx} \end{pmatrix}$. It can be expressed as a function of the director vector $\mathcal{N} = Q_{xx} + iQ_{xy} = |\mathcal{N}|e^{i\phi}$. When N rotates around the origin by an angle of θ, i.e., $\mathcal{N}' \to |\mathcal{N}|e^{i2\theta}$. Therefore, when rotated around a point by $\frac{\pi}{2}$, its sign (direction) changes. However, upon rotation by π around a point, its magnitude and direction remain unchanged except for a possible sign change, hence the name "director" or "headless vector [56]. On the other hand, under a uniform translation, the direction of the director remains unchanged. The nematic order parameter corresponds to a field that transforms under the lowest irreducible representation of the rotation group with angular momentum $l = 2$. Thus, the defined nematic phase possesses d-wave symmetry, i.e., the symmetry of quadrupoles [57]. Therefore, to quantitatively measure the nematic order after breaking the rotational symmetry, for a given state $|\psi\rangle$, we calculate the Ising nematic order parameter characterized by $d_{x^2-y^2}$ symmetry [37,58,59],

$$N_{x^2-y^2} = \frac{1}{N_e(N_e-1)} \sum_{\mathbf{q}} (\cos q_x - \cos q_y) \langle \psi | \bar{\rho}_{\mathbf{q}} \bar{\rho}_{-\mathbf{q}} | \psi \rangle, \tag{6}$$

where $\bar{\rho}_{\mathbf{q}}$ is the LLL projected guiding center density operator. This order parameter captures the anisotropy in the system. By measuring this order parameter, we can gain insight into the nature of the nematic order and its evolution as a function of various parameters, such as the strength of the magnetic field or the layer thickness. In experiments, breaking the rotational symmetry leads to anisotropic transport properties. Recently, Du *et al.* [25] observed a pronounced plasmon intensity at $\nu = 7/3$ through measurements of long-wavelength spin-wave excitations using resonant inelastic light scattering (RILS) methods in a tilted magnetic field. The plasmon intensity is proportional to the square of the plasmon coherence length. A significant peak in the coherence length indicates the presence of long-range correlations that favor translational symmetry, providing evidence for the coexistence of translational invariance and rotational symmetry breaking, namely FQHN order at $\nu = 7/3$.

For simplicity in numerical calculations, we set the z-direction frequency, ω_z, to one. We used the exact diagonalization method to determine the ground state of a finite-size system. With the ground state obtained, we then computed various physical quantities. In Fig. 4, the Ising nematic order parameters for given parameters ω_0 and ω_x at different filling factors in the 1LL are calculated. We typically

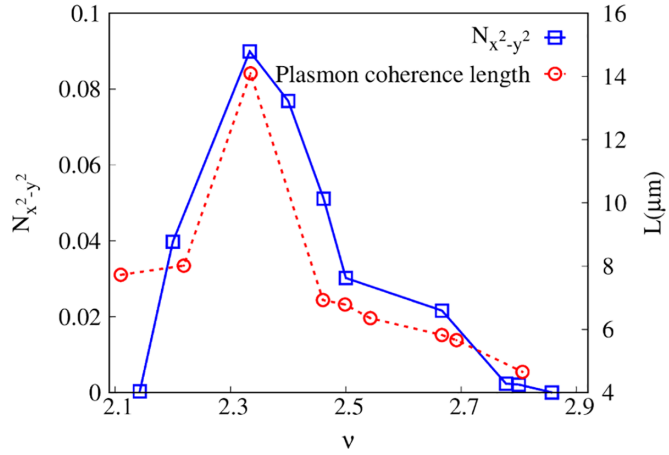

FIG. 4. For given parameters $\omega_x = 26.5$ and $\omega_0 = 1.25$, the Ising nematic order parameters $N_{x^2-y^2}$ for $7-42$ electrons at various filling factors in the 1LL are represented by the empty blue squares. The experimentally observed plasmon coherence length L in Ref. [25] is represented by the empty red circles. Both quantities exhibit peaks at $\nu = 7/3$.

select the filling factor at the incompressible states in 1LL, such as $2+1/2, 2+6/13, 2+1/3, 2+1/5$, and $2+1/7$, along with their particle-hole conjugated states which exhibit gapped ground states. Notably, when the parameters are in either the B or C phase, the value of $N_{x^2-y^2}$ consistently reaches its peak at $\nu = 7/3$. Here, the Hamiltonian includes only two-body interactions without considering the impacts from Landau-level mixing and disorder. Therefore, the system preserves the particle-hole symmetry. For instance, the wave function at $\nu = 8/3$ is identical to that at $\nu = 7/3$ after a particle-hole transformation, meaning that the $8/3$ state can be viewed as the FQH state for holes.

Nevertheless, we compute the nematic order for electrons as depicted in Eq. (6), where a larger number of electrons results in a larger denominator and thus a smaller nematic order. We expect a nematic order at $8/3$ is the same as that at $7/3$ but with the hole number N_h in Eq. (6). However, we find that the trend in the plasmon coherence length matches the order parameter Eq. (6) written for the electrons and not the equivalent one for the holes. Therefore, we use the particle hole asymmetric choice shown in Eq. (6) as the order parameter in the rest of the calculations. For comparison, we also extracted experimental data from Ref. [25] for the dependence of plasmon intensity on the filling factor. In the RILS experiment, the $7/3$ state subjected to a tilted magnetic field exhibits a large plasmon coherence length, indicating electron droplets with large translational invariance. This suggests that translational invariance and nematic order with rotational symmetry breaking can coexist in the $7/3$ state, aligning with the FQHN scenario. In our numerical calculations, we directly computed the electron nematic order and found that the $7/3$ state has the highest value compared to other filling factors in the 1LL. This implies that rotational symmetry of electrons is most fragile in the $7/3$ state in the 1LL, making it easier to form an FQHN before breaking translational symmetry. Therefore, both quantities can indicate the formation of the FQHN phase, even though they do not have a direct connection.

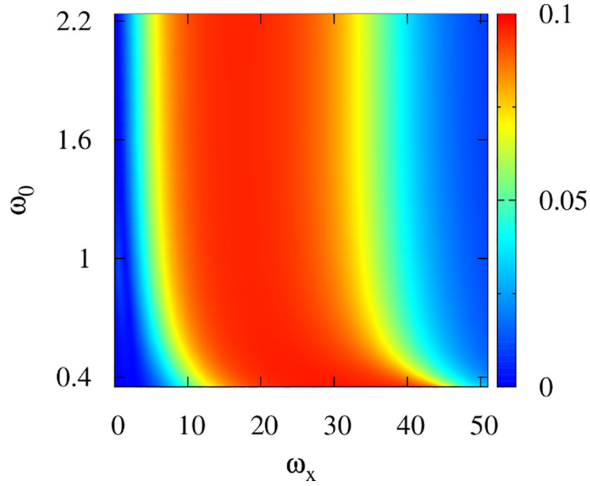

FIG. 5. The nematic order parameters of the ground state for 10 electrons at $\nu = 7/3$.

Consequently, our next analysis will concentrate mainly on the 7/3 state. By adjusting the parameters ω_x and ω_0, we computed the Ising nematic order parameters $N_{x^2-y^2}$ for the ground state with 10 electrons, and the findings are shown in Fig. 5. This approximately segments the $\omega_x - \omega_0$ plane into three regions, corresponding to the entire areas of A, B plus C, and D in Fig. 3, respectively. In the central region, it exhibits a distinct value. In phases A and D, the nematic order parameter is zero, indicating the absence of rotational symmetry breaking. In phase A, where the in-plane magnetic field is minimal, it is clearly an isotropic FQH liquid phase. Conversely, in phase D, characterized by a large in-plane magnetic field, the nematic order parameter is also zero. This can be interpreted as a CDW stripe state that lacks d-wave elliptic structure.

B. Overlap with Laughlin states

For the filling factor $\nu = 7/3$, it is reasonable to consider the Laughlin state as the model wave function when the in-plane magnetic field is small. In the isotropic case with conserved rotational symmetry, the model wave function has the well-known form $\Psi_L = \prod_{i<j}(z_i - z_j)^3 e^{-\sum_i |z_i|^2/4}$. However, it is known that the 1/3 state in the 1LL has a smaller overlap with Ψ_L than that in the LLL. Thus, to simply identify the rotational symmetry, we can compute the overlap of the wave function between the ground state and the Coulomb ground state without thickness and in-plane magnetic field in the 1LL. As depicted in Fig. 6(a), the nonzero overlap region persists only for small values of ω_x. This observation is corroborated by the Ising nematic order $N_{x^2-y^2}$ of the ground state, as shown in Fig. 5, where $N_{x^2-y^2}$ is zero. Consequently, the isotropic FQH (IFQH) phase, referred to as the A phase in Fig. 3, can be identified.

By breaking the rotational symmetry, according to Haldane's geometric explanation of the gapped FQH ground state [52], a collection of anisotropic Laughlin states can be described by an intrinsic metric. These states, denoted as $\Psi_L(g) = \prod_{i<j}[b_i^\dagger(g) - b_j^\dagger(g)]^m|0\rangle$ where $b^\dagger(g)$ is the single particle creation operator in the anisotropic Landau basis [60],

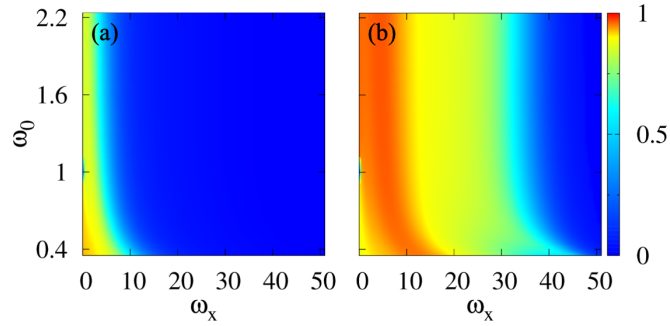

FIG. 6. In the (ω_x, ω_0) plane, (a) illustrates the overlap of the ground state wave function with that of the pure Coulomb interaction, excluding in-plane field and thickness. (b) displays the maximum overlap value between the ground state and the generalized Laughlin states, which are parameterized by varying the metric γ.

represent the unique ground state with zero energy of the model Hamiltonian with nonzero v_1. Here, g represents a unimodular metric associated with an "area preserving" deformation of the droplet

$$g = \begin{pmatrix} \cosh 2\theta + \sinh 2\theta \cos 2\phi & \sinh 2\theta \sin 2\phi \\ \sinh 2\theta \sin 2\phi & \cosh 2\theta - \sinh 2\theta \cos 2\phi \end{pmatrix},$$

where ϕ and θ represent the rotation and stretching parameters, respectively, for the primary motion of the electron in a magnetic field. By incorporating the g metric, a circular trajectory transforms into an elliptical one. In our case, we restrict the in-plane field along x direction, so the parameter ϕ should be constant. Consequently, we introduce a unified parameter $\gamma = \cosh 2\theta + \sinh 2\theta$ to characterize the metric, as discussed in the investigation of band mass anisotropy [41]. The value of $\gamma = 1$ represents the isotropic scenario with rotational symmetry. To determine the intrinsic metric γ_c of a given ground state wave function with fixed ω_x and ω_0, it is necessary to compute the overlap $\mathcal{O}_g = \mathcal{O}(\phi, \gamma) = |\langle\Psi|\Psi_L(g)\rangle|^2$, where the intrinsic metric g_c is the metric that maximizes this overlap. We produce the general Laughlin state $\Psi_L(g)$ by the effective interaction $V_{\text{eff}}(\overrightarrow{q_g}) = 2L_1(q_g^2) - 2$ which corresponds to v_1 Haldane's pseudopotential. Here, $q_g^2 = g_{ab}q^a q^b$ and $L_1(x)$ is the Laguerre polynomial. In this case, the value of g_c is consistently set to $\phi = 0$, which means that we only adjust γ within the interval of $[1, 2.5]$. Figure 6(b) shows the graph of the maximum $\mathcal{O}(\phi, \gamma)$ for the system. Since the small in-plane magnetic field region (the A phase) is isotropic, the intrinsic metric g_c in this region is an identity matrix. This suggests that the remaining region highlighted in red might indicate the anisotropic FQH phase, as optimizing the metric g can enhance the overlap to the identity, which corresponds to the B region. Here we need to note that the overlap at $\omega_x = 0$ and $\omega_0 = 0$ is not very high $|\langle\Psi|\Psi_L(g = 1)\rangle|^2 \simeq 69\%$ which means that the isotropic ground state is not very accurately described by the Laughlin state in the 1LL as mentioned previously. By increasing the layer thickness, the overlap could be significantly enhanced to ~96%, indicating that the finite layer thickness plays a role in stabilizing the Laughlin state in 1LL. A similar phenomenon was also previously observed in Ref. [61].

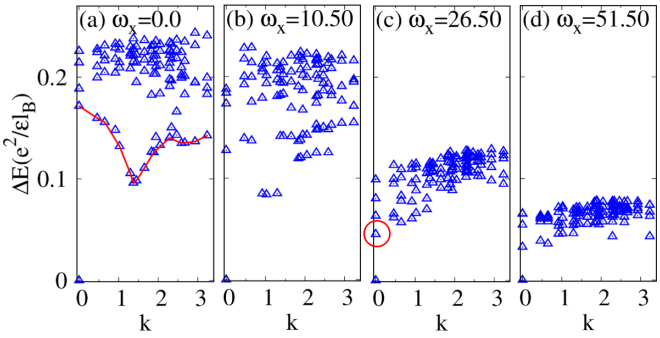

FIG. 7. The energy spectrum of 10 electrons at $\nu = 7/3$ in the 1LL, with parameters indicated by asterisks in Fig. 3. The first excited state in (c) is located in $k = 0$ subspace marked with a red circle.

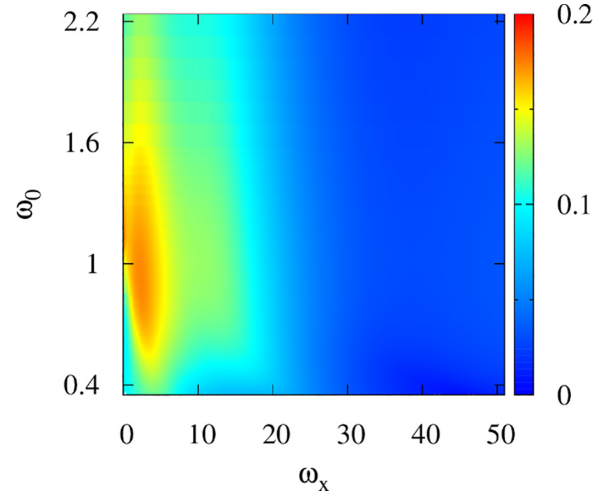

FIG. 8. The gap between the two lowest states in the $k = 0$ subspace within the (ω_x, ω_0) plane, corresponding to v_1/v_3, as illustrated in Fig. 2.

C. Energy spectrum and gap

From the previous subsection, as shown in Fig. 6(b), the region highlighted by yellow (C phase) also has a large overlap with the generalized Laughlin wave function (>80%). Moreover, both of the B and C phases have nonzero nematic order. Consequently, distinguishing between B and C based on the current results up to now is not straightforward. In order to provide more evidence for the distinguishing them, we consider the behavior of the energy gap at different regions.

To investigate the unique characteristics of different regions, we analyze their respective energy spectra and energy gaps, as shown in Fig. 7. In which we fix $\omega_0 = 1.25$ and take different values of ω_x. (a) $\omega_x = 0.0$, (b) $\omega_x = 10.5$, (c) $\omega_x = 26.5$, and (d) $\omega_x = 51.5$ represent four points (marked by stars in Fig. 3 in phases A, B, C, and D, respectively). In a finite-size system with Coulomb interaction, the magnetoroton mode is not very distinct. However, it is established that magnetoroton excitation represents the unique lowest energy excitation in the bulk, characterized by a nonzero momentum ($k \sim 1.4$) in the isotropic case, as illustrated in Fig. 7(a). The magnetoroton mode at $k = 0$ is significantly higher in energy. As the in-plane magnetic field increases, the energy of the first excited state at $k = 0$ gradually decreases and eventually becomes the global lowest excited state in Fig. 7(c). In this scenario, if the lowest bulk excitation remains the magnetoroton mode, the first excited state in the $k = 0$ space corresponds to the magnetoroton mode in the long-wavelength limit. Thus, we can say that the magnetoroton mode softens with the increasing in-plane field. Similar behavior has also been observed in a model Hamiltonain recently in Ref. [39].

We simply define the neutral gap as the spectrum gap between the ground state and the first excited state in the $k = 0$ subspace. The results for a system with 10 electrons in the $\omega_x - \omega_0$ plane are illustrated in Fig. 8. It shows that the gap is nonzero when ω_x is small and there is a maximum value for finite ω_x, which is consistent with the pseudopotential v_1/v_3 as shown in Fig. 2. It is clear that the magnetoroton mode [62–65] becomes softer as the in-plane magnetic field increases, and the lowest excited state transitions to the $k = 0$ subspace in the C and D phase, although an energy gap still remains in a finite system. To determine if the neutral gap has been eliminated, it is necessary to perform an extrapolation in the thermodynamic limit. In the following, we calculate the thermodynamic limit gap from analyzing the thermoelectric Hall conductivity scaling.

Thermoelectric effects, which allow the direct transformation of heat energy into electrical power, are both fascinating and useful. In a thermoelectric experiment, a temperature gradient ∇T is established, causing the system to generate an electrical current I to counteract its effect. The relationship between them is described by $I_i = -\alpha_{ij}\nabla_j T$, where α_{ij} denotes the thermoelectric conductivity. In practical trials, it is typical to determine the thermopower S_{xx} and Nernst coefficient S_{xy}, which are linked to α_{ij} by the equation $S_{ik} = \alpha_{ij}\rho_{jk}$, where ρ signifies resistivity. In the investigation conducted by Sheng and Fu [66], the α_{xy} was calculated for the FQH system in torus geometry. They observed a non-Fermi liquid power-law trend where α_{xy} varies as T^η with η approximately equal to 0.5 for the Fermi-liquid composite states at $\nu = 1/2$ and $\nu = 1/4$. For the Laughlin FQH state at $\nu = 1/3$, it was determined that α_{xy} decreases exponentially as $\alpha_{xy} \sim \exp(-\Delta E/k_B T)$ with a neutral magnetoroton gap as the temperature nears zero. We conducted a comparable analysis of fast-rotating dipolar fermions in the FQH regime [67]. Here, we analyze the thermoelectric Hall conductivity scaling at the same place in parameter space as that in Fig. 7. Figure 9(a) illustrates the variation in the size of the gap ΔE across various system sizes. The gap for each system is extrapolated from the scaling behavior of α_{xy} as varying the temperature as shown in Figs. 9(b) and 9(c). Therefore, the thermodynamic limit extrapolation indicates that the A/B phases exhibit a gap, whereas the C/D phases do not. However, in phase D, there is still a very small energy gap for finite systems, and thus the fitting of the exponents is still satisfied.

D. Correlation function and guiding center structure factor

For the D phase in previous studies, all the quantities, such as the nematic order, wave-function overlap, and energy gap, are zero. To acquire additional details of these phases, especially the CDW state in D phase, here we calculate the

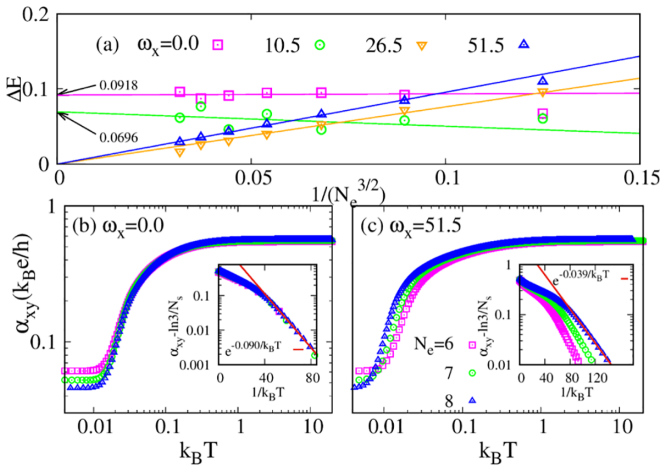

FIG. 9. (a) Finite-size scalings of the energy gap at parameters in four phases. (b) and (c) display the thermoelectric Hall conductivity α_{xy} as varying the temperature for $6-8$ electrons. In the inset of (b) and (c), the low-temperature data is fitted using the relation $\alpha_{xy} \propto \exp(-\Delta E/k_B T)$, allowing us to determine the energy gap ΔE.

pair correlation function as defined by

$$g(\mathbf{r}) = \frac{L_x L_y}{N_e(N_e-1)} \sum_{i\neq j} \langle \psi | \delta(\mathbf{r} - \mathbf{r_i} + \mathbf{r_j}) | \psi \rangle. \tag{7}$$

In Fig. 10, the $g(\mathbf{r})$ values are plotted in four phases along the x and y directions, respectively. In phase A, the pair correlation functions show symmetry for $\omega_x = 0.0$, indicating rotational symmetry. The lack of symmetry becomes more noticeable in phases B, C, and D. In particular, the values of $g(\mathbf{r})$ along the direction of y are almost identical in the anisotropic phases. In phase D, the pair correlation function along the x direction shows a nearly periodic oscillation pattern, a characteristic feature of the CDW state.

As an extra diagnostic tool for the phases of state, it is useful to consider the LLL projected guiding center static structure factor, which is actually the Fourier transformation of the pair correlation function:

$$S_0(\mathbf{q}) = \frac{1}{N_e} \sum_{i,j} \langle e^{i\mathbf{q}\cdot\mathbf{r_i}} e^{-i\mathbf{q}\cdot\mathbf{r_j}} \rangle. \tag{8}$$

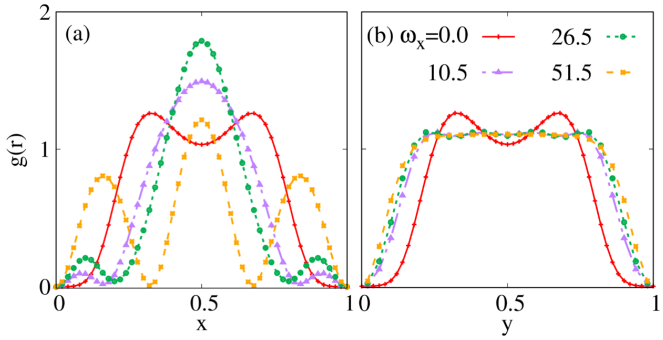

FIG. 10. The ground state pair correlation function $g(\mathbf{r})$ along the (a) x and (b) y directions with parameters indicated by stars in Fig. 3.

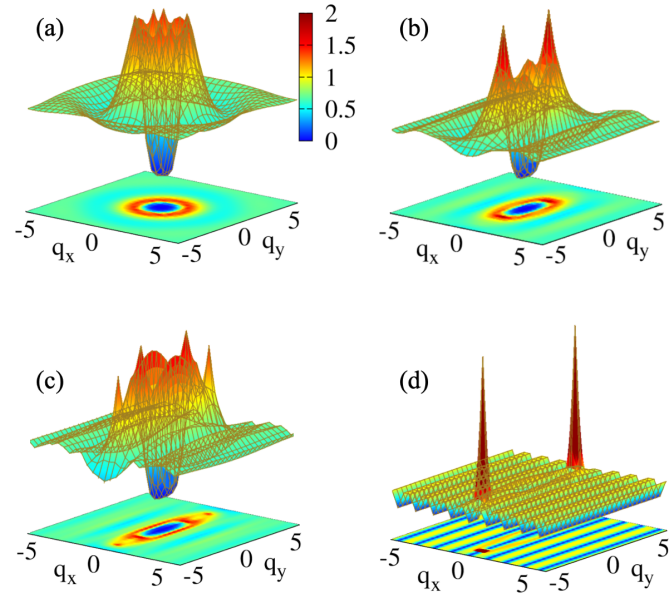

FIG. 11. The static structure factor $S_0(\mathbf{q})$ with parameters indicated by stars in Fig. 3.

The results are shown in Fig. 11 also for the same parameters as above in each phase. The transition from a circular to an elliptical contour of $S_0(\mathbf{q})$ indicates the breakdown of rotational symmetry. In Fig. 11(a), it is expected that the $S_0(\mathbf{q})$ exhibits symmetry in two directions, and a behavior proportional to q^4 near the point $q = 0$ indicates the presence of an incompressible state with a gap. In Fig. 11(b), despite the distinct appearance of $S_0(\mathbf{q})$ in two orientations, its behavior close to $q = 0$ is also quartic, suggesting the presence of a gapped anisotropic FQH state. Two sharp peaks appear in rest phases, and they become more and more prominent as increasing the in-plane field. This is similar to those previously identified in $n \geqslant 2$ LL states [68], which are the hallmark of CDW order. In particular, the phase D depicted in Fig. 11(d), the two peaks are divergent, and the remaining portion of $S_0(\mathbf{q})$ are suppressed to almost zero, suggesting that the system has transitioned into a fully 1D crystalline state. Those q values of the peaks give the length scale of the unit cell in the CDW phase.

To learn more about the CDW phase, we plot the 2D projection of $S_0(\mathbf{q})$ for several Laughlin fillings $\nu = 1/(2n+1)$ with a large in-plane magnetic field. As illustrated in Fig. 12, it is interesting to observe that there are $2n$ peaks evenly distributed along a line centered at $q = 0$. This is strongly suggestive of a tendency toward CDW ordering, as a CDW responds strongly to an external potential modulation with a wave vector that matches one of its reciprocal lattice vectors. The fact that other peaks appear only at integer multiples of the primary wave vector suggests that the CDW has a 1D structure. This is quit nature since we apply the in-plane in one direction. Similar phenomena were also previously observed in Landau levels $n \geqslant 2$ at half filling [68].

IV. SUMMARIES AND CONCLUSIONS

In this work, we investigate the fate of the FQH states in a realistic model considering the effects of the layer thickness

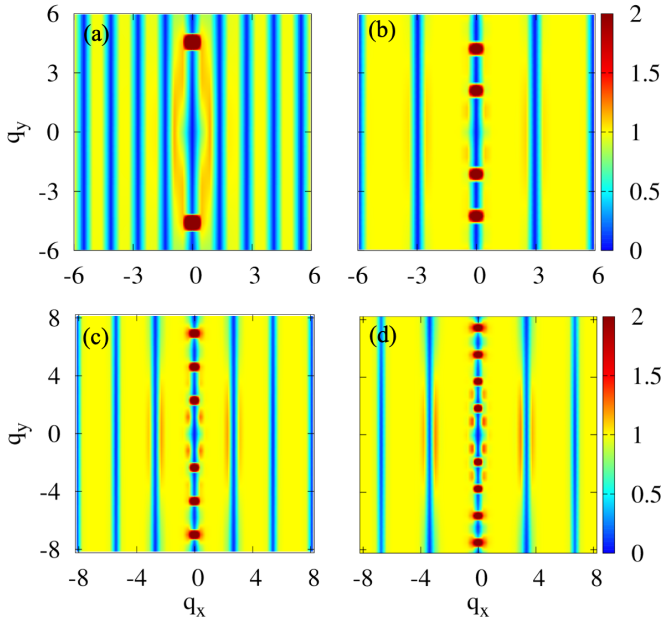

FIG. 12. The 2D plot of the static structure factor for the Laughlin filling $\nu = \frac{1}{2n+1}$ $(n = 1, 2, 3, 4)$ on the 1LL in parameterized in D phase.

and an in-plane magnetic field. Based on solving the single particle problem in this case, the electron-eletron interaction could be expressed in generalized pseudopotentials. After comparing several FQH states in the 1LL, we find that the Ising nematic order reaches its peak at $\nu = 7/3$. By adjusting the parameters ω_0 and ω_x, which represent the layer thickness and in-plane magnetic field, respectively, we calculate the Ising nematic order, wave function overlap, energy gap, pair correlation function, and the static structure factor. Finally, we arrived at the schematic phase diagram illustrated in Fig. 3. Initially, phase A exhibits an IFQH. By computing the overlap with the isotropic FQH state, we confirm the high symmetry of phase A. Furthermore, the unclosed energy gap and the Ising nematic order parameter that is essentially zero further validate the isotropic topological phase characteristics of phase A. Subsequently, phase B demonstrates an AFQH. Unlike phase A, phase B maintains an unclosed energy gap, yet its structural factors, correlation functions, and nematic order parameters exhibit distinct anisotropic features. Furthermore, the overlap between phase B and the generalized Laughlin state is remarkably high, reaching 96%. Next, phase C is identified as a FQHN. Numerical analysis reveals that the rotational symmetry of phase C is broken due to a nonzero Ising nematic order. As the in-plane magnetic field increases, the roton minimum corresponding to $k \approx 1.4$ gradually changes to $k = 0$. Moreover, in the long-wavelength limit, the energy gap at $k \to 0$ decreases, even closing in the thermodynamic limit. Finally, phase D exhibits the characteristics of a CDW. The CDW phase is characterized by a periodic oscillation pattern of the pair correlation function and sharp peaks in static structure factor. These findings align with recent resonant inelastic light scattering experimental observations and provide valuable insights into the underlying physics of the FQH states in microscopic Hamiltonians. During the manuscript preparation, we came across a recent study by Ref. [39] that introduced a microscopic model for FQHN. This model demonstrates the FQH-FQHN-CDW transition by adjusting the shortest-range pseudopotential (v_0 for bosons and v_1 for fermions) of the Coulomb interaction in the LLL. We argue that transitioning to the 1LL represents a natural approach to reduce the strength of the shortest-range pseudopotential compared to the LLL. In our approach, the phase of the fractional quantum Hall nematics is induced by an in-plane magnetic field rather than occurring spontaneously. Our discoveries could provide insight for similar experiments, particularly those involving tilted fields.

ACKNOWLEDGMENTS

This work was supported by National Natural Science Foundation of China Grants No. 12474140 and No. 12347101, the Chongqing Research Program of Basic Research and Frontier Technology Grant No. cstc2021jcyjmsxmX0081, Chongqing Talents: Exceptional Young Talents Project No. cstc2021ycjh-bgzxm0147 and the Fundamental Research Funds for the Central Universities Grant No. 2024CDJXY022.

[1] D. C. Tsui, H. L. Stormer, and A. C. Gossard, Two-dimensional magnetotransport in the extreme quantum limit, Phys. Rev. Lett. **48**, 1559 (1982).
[2] R. Prange and S. Girvin, *The Quantum Hall Effect*, *Graduate-Texts in Contemporary Physics* (Springer-Verlag, Berlin, 1987).
[3] R. B. Laughlin, Anomalous quantum Hall effect: An incompressible quantum fluid with fractionally charged excitations, Phys. Rev. Lett. **50**, 1395 (1983).
[4] E. Fradkin and S. A. Kivelson, Liquid-crystal phases of quantum Hall systems, Phys. Rev. B **59**, 8065 (1999).
[5] E. Fradkin, S. A. Kivelson, E. Manousakis, and K. Nho, Nematic phase of the two-dimensional electron gas in a magnetic field, Phys. Rev. Lett. **84**, 1982 (2000).
[6] L. Radzihovsky and A. T. Dorsey, Theory of quantum Hall nematics, Phys. Rev. Lett. **88**, 216802 (2002).
[7] K. Sun, B. M. Fregoso, M. J. Lawler, and E. Fradkin, Fluctuating stripes in strongly correlated electron systems and the nematic-smectic quantum phase transition, Phys. Rev. B **78**, 085124 (2008).
[8] D. G. Barci and E. Fradkin, Theory of the quantum Hall smectic phase. II. Microscopic theory, Phys. Rev. B **65**, 245320 (2002).
[9] M. J. Lawler and E. Fradkin, Quantum Hall smectics, sliding symmetry, and the renormalization group, Phys. Rev. B **70**, 165310 (2004).
[10] A. M. Ettouhami, C. B. Doiron, F. D. Klironomos, R. Cote, and A. T. Dorsey, Anisotropic states of two-dimensional electrons in high magnetic fields, Phys. Rev. Lett. **96**, 196802 (2006).

[11] K. Tsuda, N. Maeda, and K. Ishikawa, Anisotropic ground states of the quantum Hall system with currents, Phys. Rev. B **76**, 045334 (2007).

[12] Q. Qian, J. Nakamura, S. Fallahi, G. C. Gardner, and M. J. Manfra, Possible nematic to smectic phase transition in a two-dimensional electron gas at half-filling, Nat. Commun. **8**, 1536 (2017).

[13] L. Balents, Spatially ordered fractional quantum Hall states, Europhys. Lett. **33**, 291 (1996).

[14] J. Xia, J. P. Eisenstein, L. N. Pfeiffer, and K. W. West, Evidence for a fractionally quantized Hall state with anisotropic longitudinal transport, Nat. Phys. **7**, 845 (2011).

[15] X. Fu, Q. Shi, M. A. Zudov, G. C. Gardner, J. D. Watson, M. J. Manfra, K. W. Baldwin, L. N. Pfeiffer, and K. W. West, Anomalous nematic states in high half-filled Landau levels, Phys. Rev. Lett. **124**, 067601 (2020).

[16] M. P. Lilly, K. B. Cooper, J. P. Eisenstein, L. N. Pfeiffer, and K. W. West, Evidence for an anisotropic state of two-dimensional electrons in high Landau levels, Phys. Rev. Lett. **82**, 394 (1999).

[17] J. Xia, V. Cvicek, J. P. Eisenstein, L. N. Pfeiffer, and K. W. West, Tilt-induced anisotropic to isotropic phase transition at $\nu = 5/2$, Phys. Rev. Lett. **105**, 176807 (2010).

[18] Y. Liu, S. Hasdemir, M. Shayegan, L. N. Pfeiffer, K. W. West, and K. W. Baldwin, Evidence for a $\nu = 5/2$ fractional quantum Hall nematic state in parallel magnetic fields, Phys. Rev. B **88**, 035307 (2013).

[19] M. S. Hossain, M. K. Ma, Y. J. Chung, S. K. Singh, A. Gupta, K. W. West, K. W. Baldwin, L. N. Pfeiffer, R. Winkler, and M. Shayegan, Valley-tunable even-denominator fractional quantum Hall state in the lowest Landau level of an anisotropic system, Phys. Rev. Lett. **130**, 126301 (2023).

[20] M. S. Hossain, M. K. Ma, Y. J. Chung, L. N. Pfeiffer, K. W. West, K. W. Baldwin, and M. Shayegan, Unconventional anisotropic even-denominator fractional quantum Hall state in a system with mass anisotropy, Phys. Rev. Lett. **121**, 256601 (2018).

[21] M. Shayegan, E. P. D. Poortere, O. Gunawan, Y. P. Shkolnikov, E. Tutuc, and K. Vakili, Two-dimensional electrons occupying multiple valleys in AlAs, Phys. Status Solidi B **243**, 3629 (2006).

[22] N. Samkharadze, K. A. Schreiber, G. C. Gardner, M. J. Manfra, E. Fradkin, and G. A. Csáthy, Observation of a transition from a topologically ordered to a spontaneously broken symmetry phase, Nat. Phys. **12**, 191 (2016).

[23] K. A. Schreiber, N. Samkharadze, G. C. Gardner, R. R. Biswas, M. J. Manfra, and G. A. Csáthy, Onset of quantum criticality in the topological-to-nematic transition in a two-dimensional electron gas at filling factor $\nu = 5/2$, Phys. Rev. B **96**, 041107(R) (2017).

[24] K. A. Schreiber, N. Samkharadze, G. C. Gardner, Y. L. Geller, M. J. Manfra, L. N. Pfeiffer, K. W. West, and G. A. Csáthy, Electron-electron interactions and the paired-to-nematic quantum phase transition in the second Landau level, Nat. Commun. **9**, 2400 (2018).

[25] L. Du, U. Wurstbauer, K. W. West, L. N. Pfeiffer, S. Fallahi, G. C. Gardner, M. J. Manfra, and A. Pinczuk, Observation of new plasmons in the fractional quantum Hall effect: Interplay of topological and nematic orders, Sci. Adv. **5**, eaav3407 (2019).

[26] A. A. Koulakov, M. M. Fogler, and B. I. Shklovskii, Charge density wave in two-dimensional electron liquid in weak magnetic field, Phys. Rev. Lett. **76**, 499 (1996).

[27] M. M. Fogler, A. A. Koulakov, and B. I. Shklovskii, Ground state of a two-dimensional electron liquid in a weak magnetic field, Phys. Rev. B **54**, 1853 (1996).

[28] A. H. MacDonald and M. P. A. Fisher, Quantum theory of quantum Hall smectics, Phys. Rev. B **61**, 5724 (2000).

[29] M. M. Fogler, Quantum Hall liquid crystals, Int. J. Mod. Phys. B **16**, 2924 (2002).

[30] D. G. Barci, E. Fradkin, S. A. Kivelson, and V. Oganesyan, Theory of the quantum Hall smectic Phase. I. Low-energy properties of the quantum Hall smectic fixed point, Phys. Rev. B **65**, 245319 (2002).

[31] S. Y. Lee, V. W. Scarola, and J. K. Jain, Structures for interacting composite fermions: Stripes, bubbles, and fractional quantum Hall effect, Phys. Rev. B **66**, 085336 (2002).

[32] M. Mulligan, C. Nayak, and S. Kachru, Isotropic to anisotropic transition in a fractional quantum Hall state, Phys. Rev. B **82**, 085102 (2010).

[33] M. Mulligan, C. Nayak, and S. Kachru, Effective field theory of fractional quantized Hall nematics, Phys. Rev. B **84**, 195124 (2011).

[34] J. Maciejko, B. Hsu, S. A. Kivelson, Y. J. Park, and S. L. Sondhi, Field theory of the quantum Hall nematic transition, Phys. Rev. B **88**, 125137 (2013).

[35] Y. You, G. Y. Cho, and E. Fradkin, Theory of nematic fractional quantum Hall states, Phys. Rev. X **4**, 041050 (2014).

[36] B. Yang, Microscopic theory for nematic fractional quantum Hall effect, Phys. Rev. Res. **2**, 033362 (2020).

[37] N. Regnault, J. Maciejko, S. A. Kivelson, and S. L. Sondhi, Evidence of a fractional quantum Hall nematic phase in a microscopic model, Phys. Rev. B **96**, 035150 (2017).

[38] T. Graß, P. Bienias, M. J. Gullans, R. Lundgren, J. Maciejko, and A. V. Gorshkov, Fractional quantum Hall phases of Bosons with tunable interactions: From the Laughlin liquid to a fractional Wigner crystal, Phys. Rev. Lett. **121**, 253403 (2018).

[39] S. Pu, A. C. Balram, J. Taylor, E. Fradkin, and Z. Papic, Microscopic model for fractional quantum Hall nematics, Phys. Rev. Lett. **132**, 236503 (2024).

[40] H. Wang, R. Narayanan, X. Wan, and F. Zhang, Fractional quantum Hall states in two-dimensional electron systems with anisotropic interactions, Phys. Rev. B **86**, 035122 (2012).

[41] B. Yang, Z. Papić, E. H. Rezayi, R. N. Bhatt, and F. D. M. Haldane, Band mass anisotropy and the intrinsic metric of fractional quantum Hall systems, Phys. Rev. B **85**, 165318 (2012).

[42] E. H. Rezayi and F. D. M. Haldane, Incompressible paired Hall state, stripe order, and the composite fermion liquid phase in half-filled Landau levels, Phys. Rev. Lett. **84**, 4685 (2000).

[43] W. N. Faugno, T. Zhao, A. C. Balram, T. Jolicoeur, and J. K. Jain, Unconventional $\mathbb{Z}_n$ parton states at $\nu = 7/3$: Role of finite width, Phys. Rev. B **103**, 085303 (2021).

[44] L. P. Yang, Q. Li, and Z. X. Hu, Behavior of fractional quantum Hall states in LLL and 1LL with in-plane magnetic field and Landau level mixing: A numerical investigation, Chin. Phys. B **27**, 087306 (2018).

[45] G. Moore and N. Read, Nonabelions in the fractional quantum Hall effect, Nucl. Phys. B **360**, 362 (1991).

[46] R. H. Morf, Transition from quantum Hall to compressible states in the second Landau level: New light on the $\nu = 5/2$ enigma, Phys. Rev. Lett. **80**, 1505 (1998).

[47] A. Stern, Non-Abelian states of matter, Nature (London) **464**, 187 (2010).

[48] C. Nayak, S. H. Simon, A. Stern, M. Freedman, and S. D. Sarma, Non-Abelian anyons and topological quantum computation, Rev. Mod. Phys. **80**, 1083 (2008).

[49] W. Pan, R. R. Du, H. L. Stormer, D. C. Tsui, L. N. Pfeiffer, K. W. Baldwin, and K. W. West, Strongly anisotropic electronic transport at Landau level filling factor $\nu = 9/2$ and $\nu = 5/2$ under a tilted magnetic field, Phys. Rev. Lett. **83**, 820 (1999).

[50] J. P. Eisenstein, R. Willett, H. L. Stormer, D. C. Tsui, A. C. Gossard, and J. H. English, Collapse of the even-denominator fractional quantum Hall effect in tilted fields, Phys. Rev. Lett. **61**, 997 (1988).

[51] B. Friess, V. Umansky, L. Tiemann, K. von Klitzing, and J. H. Smet, Probing the microscopic structure of the stripe phase at filling factor 5/2, Phys. Rev. Lett. **113**, 076803 (2014).

[52] F. D. M. Haldane, Geometrical description of the fractional quantum Hall effect, Phys. Rev. Lett. **107**, 116801 (2011).

[53] B. Yang, Z. X. Hu, C. H. Lee, and Z. Papic, Generalized pseudopotentials for the anisotropic fractional quantum Hall effect, Phys. Rev. Lett. **118**, 146403 (2017).

[54] B. Yang, C. H. Lee, C. Zhang, and Z. X. Hu, Anisotropic pseudopotential characterization of quantum Hall systems under a tilted magnetic field, Phys. Rev. B **96**, 195140 (2017).

[55] C. R. Dean, B. A. Piot, P. Hayden, S. D. Sarma, G. Gervais, L. N. Pfeiffer, and K. W. West, Contrasting behavior of the $\frac{5}{2}$ and $\frac{7}{3}$ fractional quantum Hall effect in a tilted field, Phys. Rev. Lett. **101**, 186806 (2008).

[56] P. G. de Gennes and J. Prost, *The Physics of Liquid Crystals* (Clarendon, Oxford, 1993).

[57] E. Fradkin, *Electronic Liquid Crystal Phases in Strongly Correlated Systems, Lecture Notes in Physics* Vol. 843, edited by D. C. Cabra, A. Honecker, and P. Pujol (Springer-Verlag, Berlin, 2012).

[58] D. A. Abanin, S. A. Parameswaran, S. A. Kivelson, and S. L. Sondhi, Nematic valley ordering in quantum Hall systems, Phys. Rev. B **82**, 035428 (2010).

[59] M. A. Metlitski and S. Sachdev, Quantum phase transitions of metals in two spatial dimensions. I. Ising-nematic order, Phys. Rev. B **82**, 075127 (2010).

[60] R. Z. Qiu, F. D. M. Haldane, X. Wan, K. Yang, and S. Yi, Model anisotropic quantum Hall states, Phys. Rev. B **85**, 115308 (2012).

[61] M. R. Peterson, T. Jolicoeur, and S. Das Sarma, Orbital Landau level dependence of the fractional quantum Hall effect in quasi-two-dimensional electron layers: Finite-thickness effects, Phys. Rev. B **78**, 155308 (2008).

[62] A. Pinczuk, B. S. Dennis, L. N. Pfeiffer, and K. West, Observation of collective excitations in the fractional quantum Hall effect, Phys. Rev. Lett. **70**, 3983 (1993).

[63] M. Kang, A. Pinczuk, B. S. Dennis, L. N. Pfeiffer, and K. W. West, Observation of multiple magnetorotons in the fractional quantum Hall effect, Phys. Rev. Lett. **86**, 2637 (2001).

[64] I. V. Kukushkin, J. H. Smet, V. W. Scarola, V. Umansky, and K. von Klitzing, Dispersion of the excitations of fractional quantum Hall states, Science **324**, 1044 (2009).

[65] S. M. Girvin, A. H. MacDonald, and P. M. Platzman, Collective-excitation gap in the fractional quantum Hall effect, Phys. Rev. Lett. **54**, 581 (1985).

[66] D. N. Sheng and L. Fu, Thermoelectric response and entropy of fractional quantum Hall systems, Phys. Rev. B **101**, 241101(R) (2020).

[67] Z. Y. Fang, D. Ye, Y. Y. Zhang, and Z. X. Hu, Thermoelectric Hall conductivity of fractional quantum Hall systems on a disk, Phys. Rev. B **103**, 235161 (2021).

[68] E. H. Rezayi, F. D. M. Haldane, and K. Yang, Charge-density-wave ordering in half-filled high Landau levels, Phys. Rev. Lett. **83**, 1219 (1999).